Unresolved Transition Arrays and EUV and Soft X-ray Source Development

Gerry O'Sullivan, Padraig Dunne, Deirdre Kilbane, Rebekah D'Arcy, Bowen Li and Colm Harte
School of Physics, University College Dublin, Belfield, Dublin 4, Ireland.

Takeshi Higashiguchi, Takamitsu Otsuka and Noboru Yugami
Department of Advanced Interdisciplinary Sciences, Utsunomiya University, Yoto 7-1-2, Utsunomiya, Tochigi 321-8585 Japan

Akira Endo
HiLASE Project, Institute of Physics AS, CR, Na Slovance 2, 18221 Prague 8, Czech Republic

Outline

- Background
- Properties and applications of $\Delta n = 0$ arrays
- Properties of and applications $\Delta n = 1$ arrays
- Conclusion

Typical EUV Spectrum

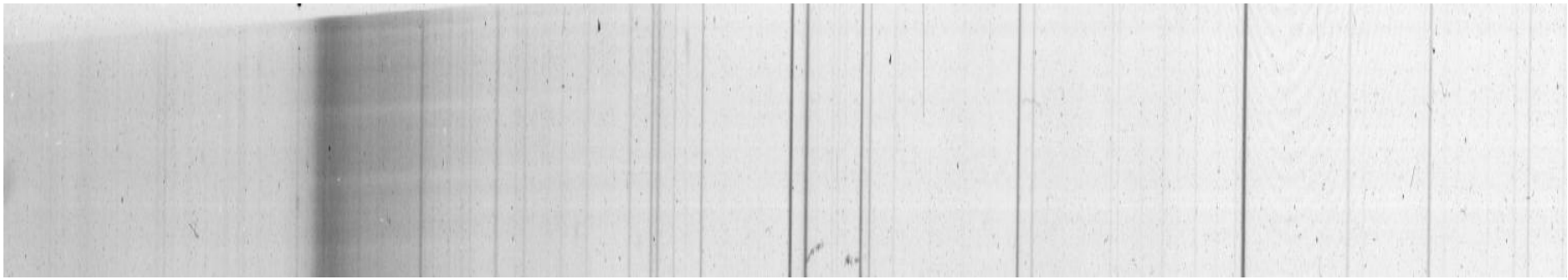

onsists of:

- Lines (bound-bound transitions), because of high density, lines from high n states are usually not seen
- Recombination Radiation (bound-free transitions) which scales as $\langle\zeta\rangle^4$ where $\langle\zeta\rangle$ is the average ionic charge
- Bremsstrahlung (free-free)

For an optically thin plasma: P_{lines}:P_{recomb}:P_{brem} = 100:10:1

In some cases lines cluster together to form a UTA (unresolved transition array)

What is a UTA?

- A UTA generally has too many lines to identify individual transitions.
- Ideally linewidth > line seperation
- Both the energy levels and spectra can be parameterised statistically in terms of moments - μ_n of the array *(Bauche, and Bauche-Arnoult Phys Scr **T40**, 58, 1992)*

$$\mu_n = \sum_{a,b} \frac{[\langle a|H|a\rangle - \langle b|H|b\rangle]^n w_{ab}}{W}$$

$$w_{ab} = |\langle a|\boldsymbol{D}|b\rangle|^2,$$

$$\boldsymbol{D} = -\Sigma_i e\boldsymbol{r}_i$$

$$W = \sum_{a,b} w_{ab}$$

- UTA described by:
  - Position - μ_1
  - Width - $\sigma = [\mu_2 - \mu_1^2]^{1/2}$

Two types of UTA in XUV spectra

Δn = 0

Increasing power density ↓

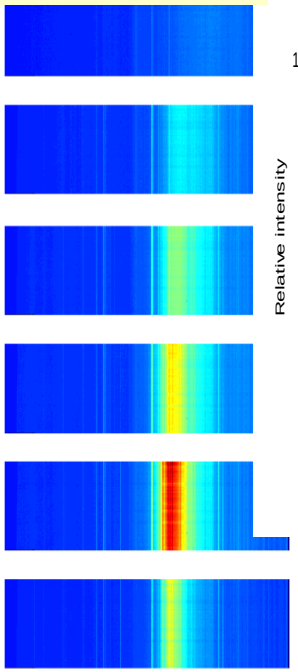

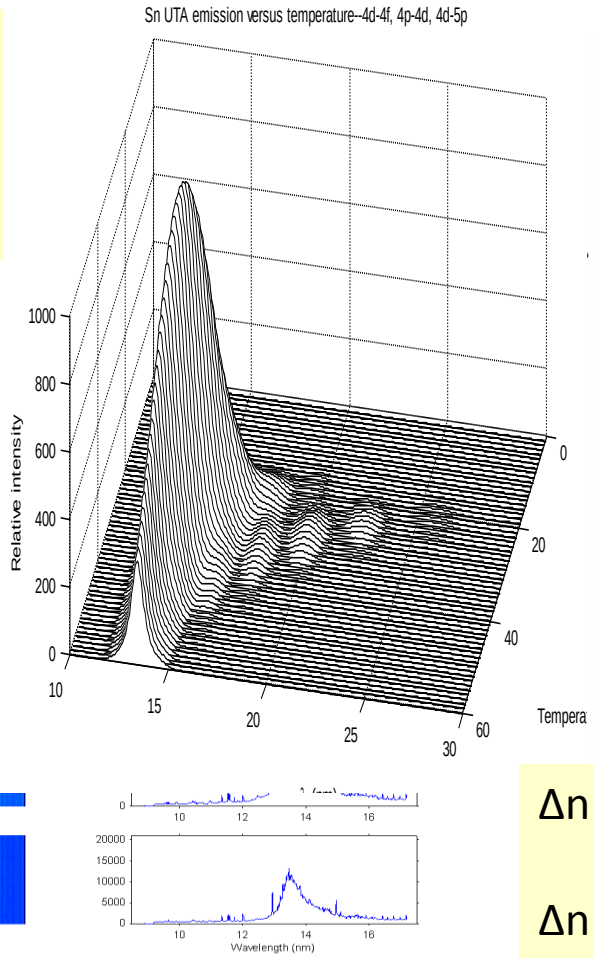

Δn = 0 n=4- n=4 transitions in a Sn plasma

Δn > 0

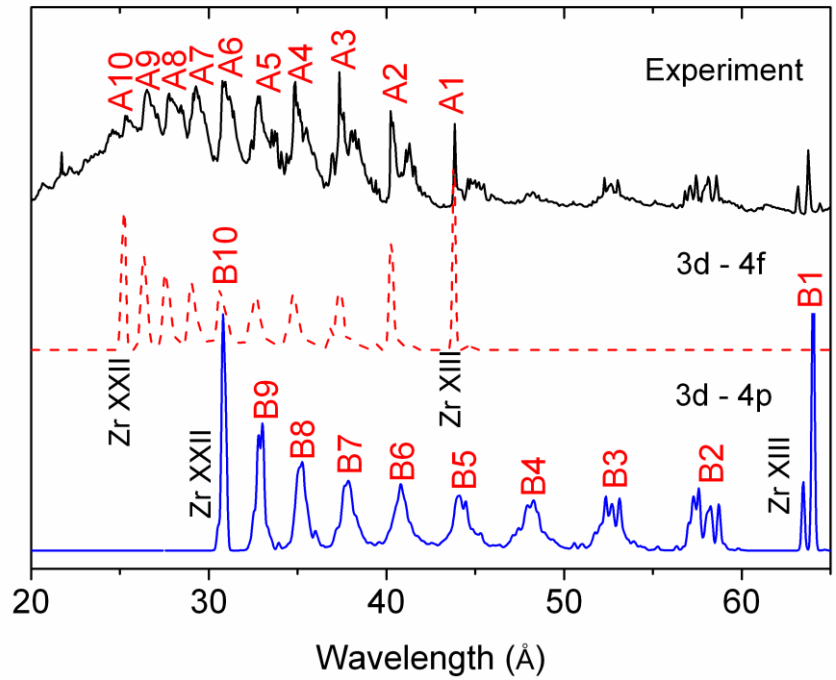

Δn = 0 transitions overlap in adjacent ion stages.

Δn = 0 transitions do not overlap in adjacent ion stages and move to shorter wavelengths with increasing ionization.

- Background and underlying theory
- Properties and applications of $\Delta n = 0$ arrays
- Properties of and applications $\Delta n = 1$ arrays
- Conclusion

Variation of UTA position with Z

UTA due to $4p^6 4d^n$ - $4p^5 4d^{n+1} + 4d^{n-1} 4f$ ($0 \leq n \leq 9$) mixed arrays.

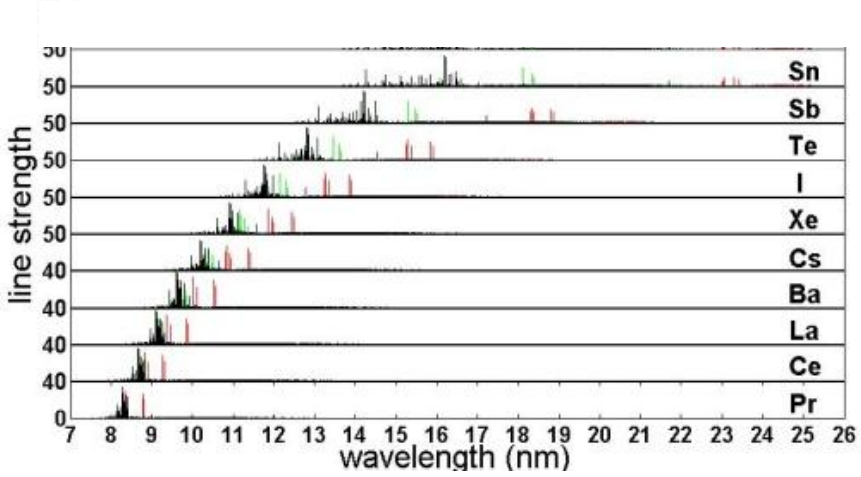

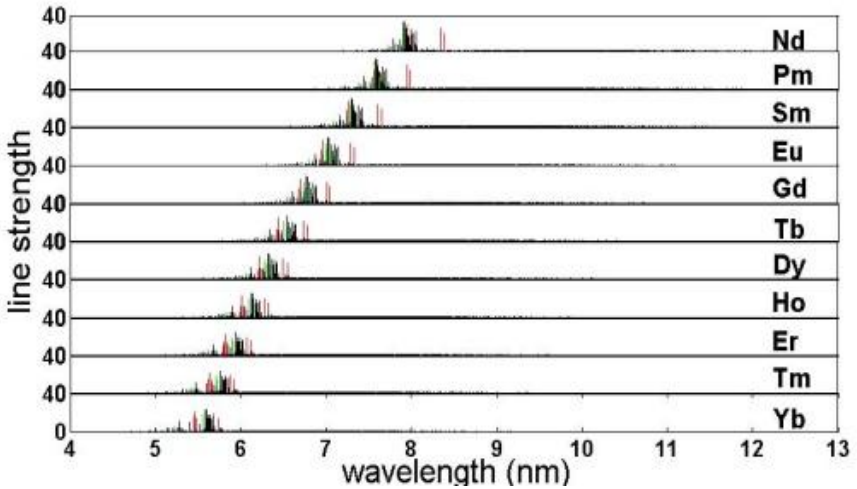

Width of UTA :
Minimum in rare earths, due to complete contraction of 4f wavefunction and almost constant value of <4d|4f> .
Broadens in very high Z due to 4d and 4p spin orbit splitting

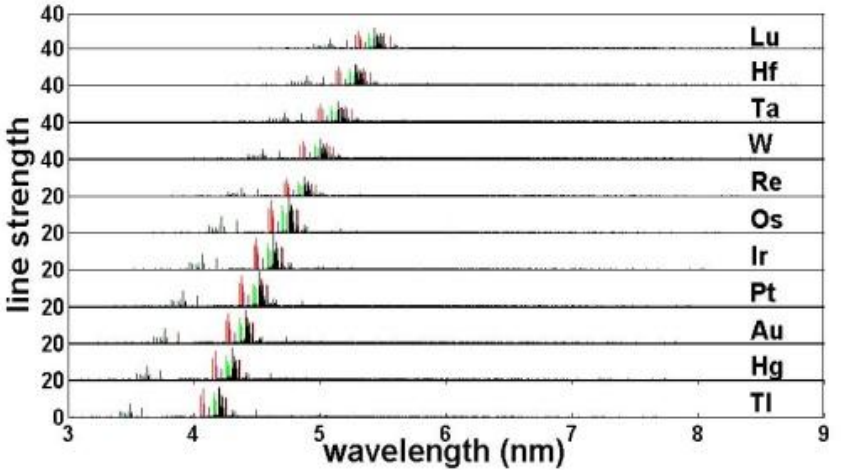

Opacity Effects

- Spectra from metal targets dominated by continuum emission

  Some strong emission and absorption lines

  Big contribution from satellite lines

- Spectra of targets with low % of element of interest dominated by an intense Unresolved Transition Array (UTA), with greatly reduced continuum emission

  Satellites unimportant because of lower ion density

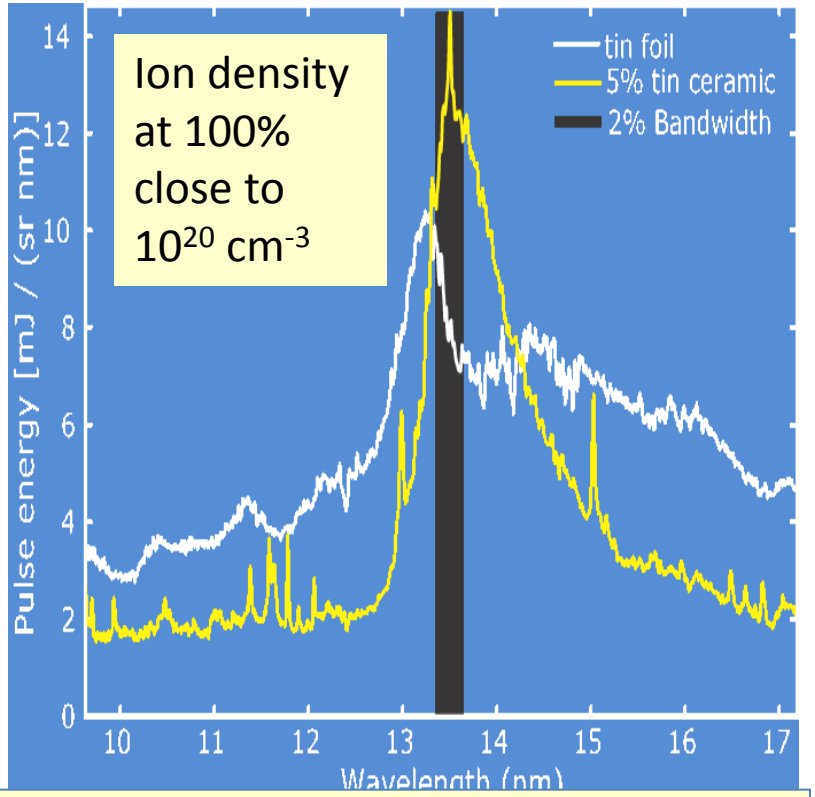

As concentration decreases:

- UTA narrows
- off-band emission decreases.
- UTA intensity grows, maximum at concentrations (by number) of ~2% - 5%.

(Hayden et al Microelectron Eng. 83, 699 2006)

Direct observation of satellites

PHYSICAL REVIEW A 79, 042509 (2009)

Transitions and the effects of configuration interaction in the spectra of Sn XV–Sn XVIII

R. D'Arcy,[1] H. Ohashi,[2] S. Suda,[2] H. Tanuma,[2] S. Fujioka,[3] H. Nishimura,[3] K. Nishihara,[3] C. Suzuki,[4] T. Kato,[4] F. Koike,[5] J. White,[1] and G. O'Sullivan[1]

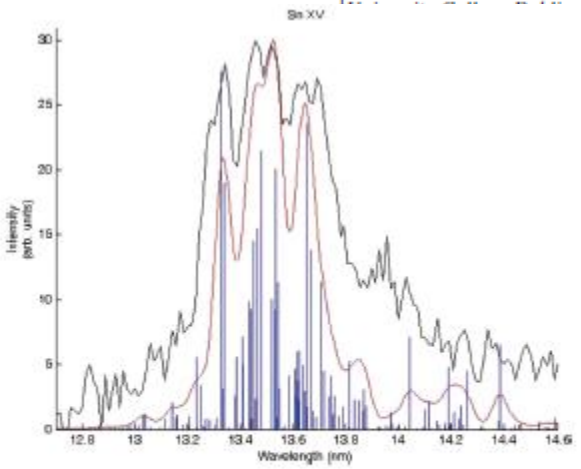

FIG. 7. (Color online) Comparison between a theoretical spectrum for Sn XV convolved with a Gaussian instrumental function and the obtained experimental spectrum of Sn XV. The theoretical data are also presented in the form of stick plots of height equal to the *gf* value.

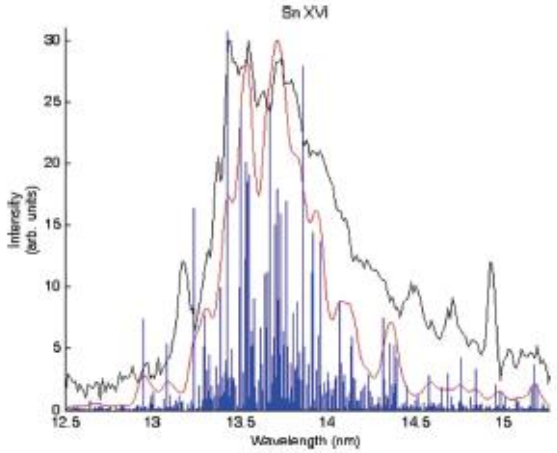

FIG. 8. (Color online) Comparison between a theoretical spectrum for Sn XVI convolved with a Gaussian instrumental function and the obtained experimental spectrum of Sn XVI. The theoretical data are also presented in the form of stick plots of height equal to the *gf* value.

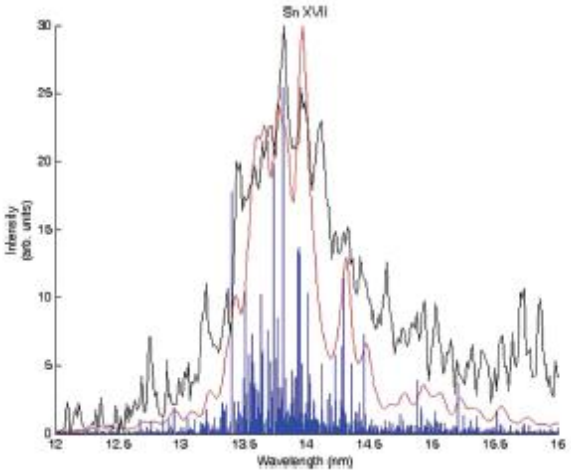

FIG. 9. (Color online) Comparison between a theoretical spectrum for Sn XVII convolved with a Gaussian instrumental function and the obtained experimental spectrum of Sn XVII. The theoretical data are also presented in the form of stick plots of height equal to the *gf* value.

In Sn XV, ground state is $4p^6$, expect $4p(^1S_0) – 4d(^1P_1)$ transition, one strong line.

Observe a UTA, due to excited to excited state (4d – 4f) transitions

Satellites due to transitions of the type

$4s^24p^n4d – 4s^24p^n4f + 4s^24p^{n-1}4d^2 + 4s4p^{n+1}4d$

Influence of source on UTA profile

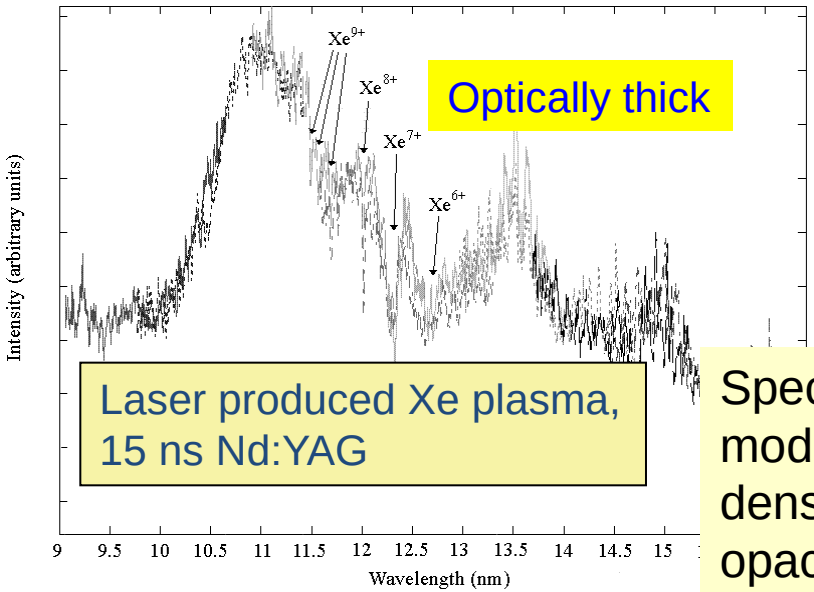

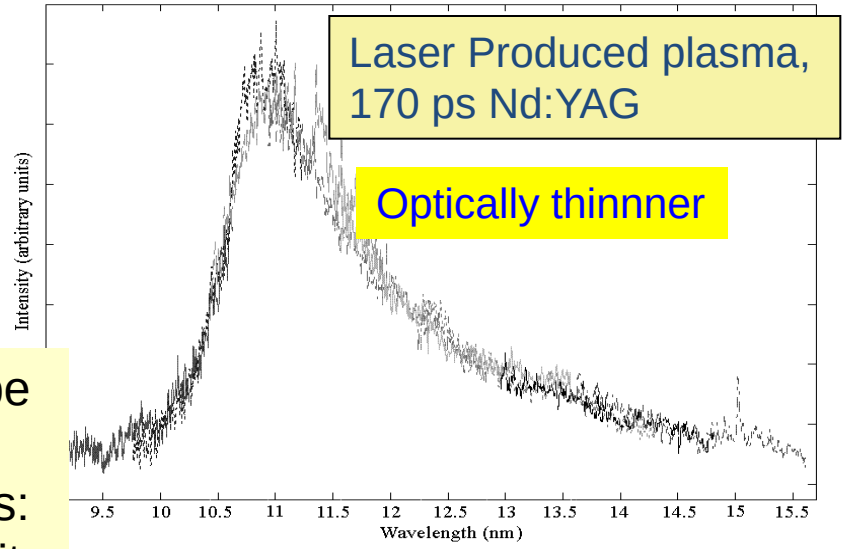

Spectral shape modified by density effects: opacity, satellite lines *(Sasaki et al. IEEE Journal of Quant. Electron.10, 1307 2004)*

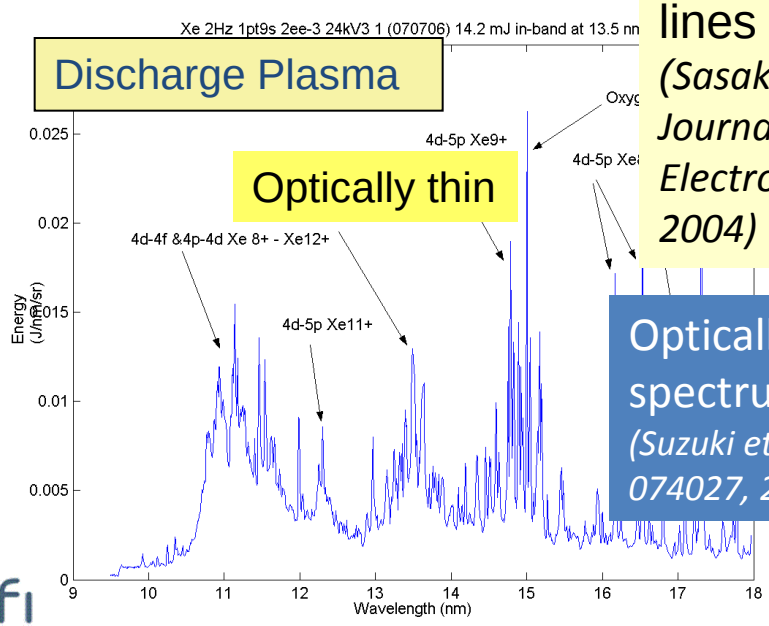

Optically thin spectrum -NIFS *(Suzuki et al JPB 4 , 074027, 2010)*

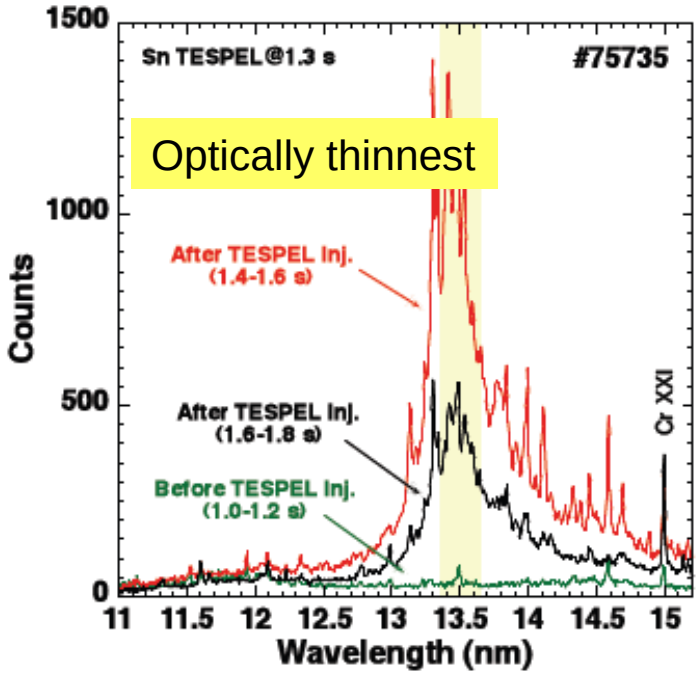

Sources @ 6.x nm

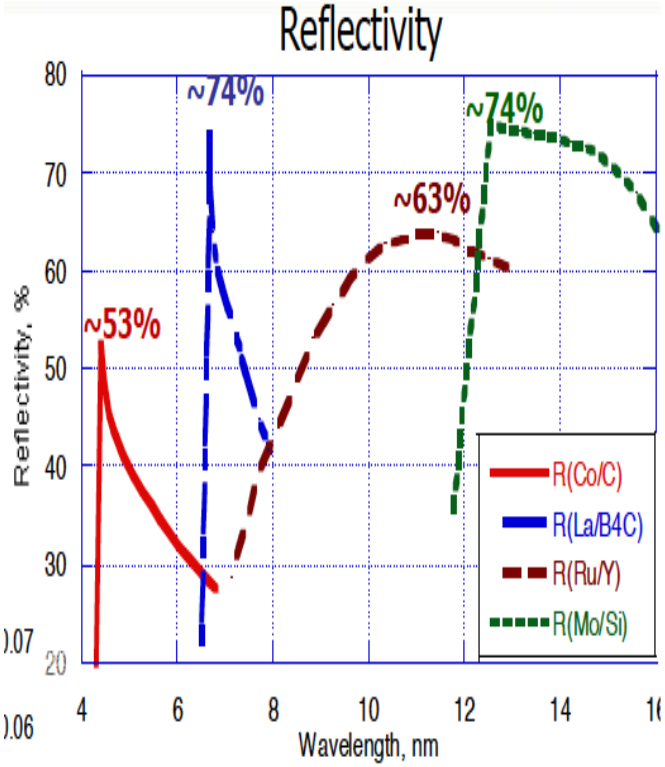

Interest in sources at 6.7 nm due to availability of Mo/B4C multilayer mirrors with a theoretical reflectivity of 74%

IOP Publishing
Physica Scripta
Phys. Scr. **80** (2009) 045303 (6pp)
doi:10.1088/0031-8949/80/04/045303

EUV spectra of Gd and Tb ions excited in laser-produced and vacuum spark plasmas

S S Churilov[1], R R Kildiyarova, A N Ryabtsev and S V Sadovsky

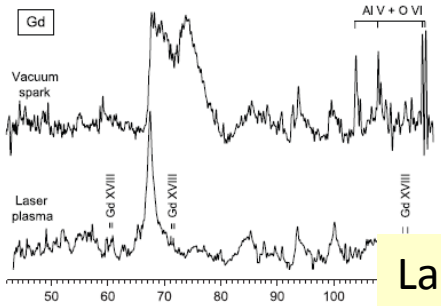

Figure 1. Spectra of gadolinium ions excited in the vacuum spark (upper trace) and in the laser-

Laser:
3 J in 20 ns
$\lambda = 1.06\ \mu m$
$\Phi = (5–8)\times10^{11}\ Wcm^{-2}$

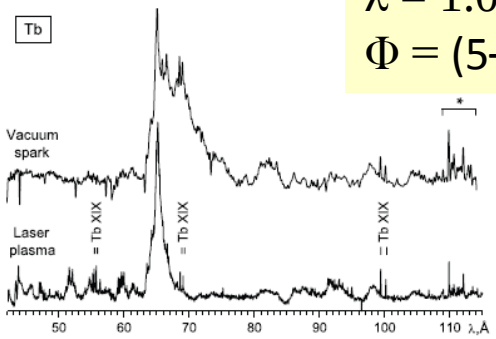

Figure 2. Spectra of terbium ions excited in the vacuum spark (upper trace) and in the laser-produced plasma (bottom trace). *, $4f^2–4f5d$ transition array in Tb XVIII classified in the present work.

The ground state problem

4f binding energy increases with ion charge faster than 5p or 5s.

4f and 5p levels cross near VIIIth spectrum, 4f and 5s cross near XIVth.

TABLE II. Ground-state configurations of ions in stages V–XVII for elements lanthanum through hafnium. Discrepancies between the current table and Table I of [22] are highlighted in bold.

	V	VI	VII	VIII	IX	X	XI	XII	XIII	XIV	XV	XVI	XVII
La	$5s^25p^5$	$5s^25p^4$	$5s^25p^3$	$5s^25p^2$	$5s^25p$	$5s^2$	$5s$	$4d^{10}$	$4d^9$	$4d^8$	$4d^7$	$4d^6$	$4d^5$
Ce	$5s^25p^6$	$5s^25p^5$	$\mathbf{5s^25p^4}$	$\mathbf{5s^25p^3}$	$\mathbf{5s^25p^2}$	$\mathbf{5s^25p}$	$5s^2$	$5s$	$4d^{10}$	$4d^9$	$4d^8$	$4d^7$	$4d^6$
Pr	$5p^64f$	$5s^25p^6$	$\mathbf{5s^25p^5}$	$\mathbf{5s^25p^4}$	$\mathbf{5s^25p^3}$	$\mathbf{5s^25p^2}$	$5s^24f$	$5s^2$	$5s$	$4d^{10}$	$4d^9$	$4d^8$	$4d^7$
Nd	$5p^64f^2$	$5p^64f$	$\mathbf{5s^25p^6}$	$\mathbf{5s^25p^5}$	$\mathbf{5p^34f}$	$\mathbf{5p^24f}$	$5s^24f^2$	$5s^24f$	$5s^2$	$5s$	$4d^{10}$	$4d^9$	$4d^8$
Pm	$5p^64f^3$	$5p^64f^2$	$\mathbf{5p^64f}$	$\mathbf{5p^54f}$	$\mathbf{5p^34f^2}$	$\mathbf{5p^24f^2}$	$5s^24f^3$	$5s^24f^2$	$5s^24f$	$5s^2$	$4f$	$4d^{10}$	$4d^9$
Sm	$5p^64f^4$	$5p^64f^3$	$\mathbf{5p^64f^2}$	$\mathbf{5p^54f^2}$	$\mathbf{5p^34f^3}$	$\mathbf{5p^24f^3}$	$5s^24f^4$	$5s^24f^3$	$5s^24f^2$	$5s^24f$	$\mathbf{5s4f}$	$4f$	$4d^{10}$
Eu	$5p^64f^5$	$5p^64f^4$	$\mathbf{5p^64f^3}$	$\mathbf{5p^54f^3}$	$\mathbf{5p^34f^4}$	$\mathbf{5p^24f^4}$	$5s^24f^5$	$5s^24f^4$	$5s^24f^3$	$5s^24f^2$	$\mathbf{5s4f^2}$	$4f^2$	$4f$
Gd	$5p^64f^6$	$5p^64f^5$	$\mathbf{5p^64f^4}$	$\mathbf{5p^54f^4}$	$\mathbf{5p^44f^4}$	$\mathbf{5p^24f^5}$	$5s^24f^6$	$5s^24f^5$	$5s^24f^4$	$5s^24f^3$	$\mathbf{5s4f^3}$	$4f^3$	$4f^2$
Tb	$5p^64f^7$	$5p^64f^6$	$\mathbf{5p^64f^5}$	$\mathbf{5p^54f^5}$	$\mathbf{5p^44f^5}$	$\mathbf{5p^24f^6}$	$5s^24f^7$	$5s^24f^6$	$5s^24f^5$	$5s^24f^4$	$\mathbf{5s4f^4}$	$4f^4$	$4f^3$
Dy	$5p^64f^8$	$5p^64f^7$	$\mathbf{5p^64f^6}$	$\mathbf{5p^54f^6}$	$\mathbf{5p^44f^6}$	$\mathbf{5p^24f^7}$	$\mathbf{5p4f^7}$	$5s^24f^7$	$5s^24f^6$	$5s^24f^5$	$\mathbf{5s^24f^4}$	$4f^5$	$4f^4$
Ho	$5p^64f^9$	$5p^64f^8$	$\mathbf{5p^64f^7}$	$\mathbf{5p^54f^7}$	$\mathbf{5p^44f^7}$	$\mathbf{5p^24f^8}$	$\mathbf{5p4f^8}$	$5s^24f^8$	$5s^24f^7$	$5s^24f^6$	$\mathbf{5s^24f^5}$	$4f^6$	$4f^5$
Er	$5p^64f^{10}$	$5p^64f^9$	$\mathbf{5p^64f^8}$	$\mathbf{5p^54f^8}$	$\mathbf{5p^44f^8}$	$\mathbf{5p^24f^9}$	$\mathbf{5p4f^9}$	$5s^24f^9$	$5s^24f^8$	$5s^24f^7$	$\mathbf{5s^24f^6}$	$\mathbf{5s4f^6}$	$4f^6$
Tm	$5p^64f^{11}$	$5p^64f^{10}$	$\mathbf{5p^64f^9}$	$\mathbf{5p^64f^8}$	$\mathbf{5p^44f^9}$	$\mathbf{5p^24f^{10}}$	$\mathbf{5p4f^{10}}$	$5s^24f^{10}$	$5s^24f^9$	$5s^24f^8$	$\mathbf{5s^24f^7}$	$\mathbf{5s4f^7}$	$4f^7$
Yb	$5p^64f^{12}$	$5p^64f^{11}$	$\mathbf{5p^64f^{10}}$	$\mathbf{5p^64f^9}$	$\mathbf{5p^44f^{10}}$	$\mathbf{5p^34f^{10}}$	$\mathbf{5p4f^{11}}$	$5s^24f^{11}$	$5s^24f^{10}$	$5s^24f^9$	$\mathbf{5s^24f^8}$	$\mathbf{5s4f^8}$	$4f^8$
Lu	$5p^64f^{13}$	$5p^64f^{12}$	$\mathbf{5p^64f^{11}}$	$\mathbf{5p^64f^{10}}$	$\mathbf{5p^44f^{11}}$	$\mathbf{5p^34f^{11}}$	$\mathbf{5p4f^{12}}$	$5s^24f^{12}$	$5s^24f^{11}$	$5s^24f^{10}$	$\mathbf{5s^24f^9}$	$\mathbf{5s4f^9}$	$4f^9$

FAC code calculations for Gd

JOURNAL OF APPLIED PHYSICS 108, 104905 (2010)

Extreme ultraviolet emission spectra of Gd and Tb ions

D. Kilbane[a] and G. O'Sullivan
School of Physics, University College Dublin, Belfield, Dublin 4, Ireland

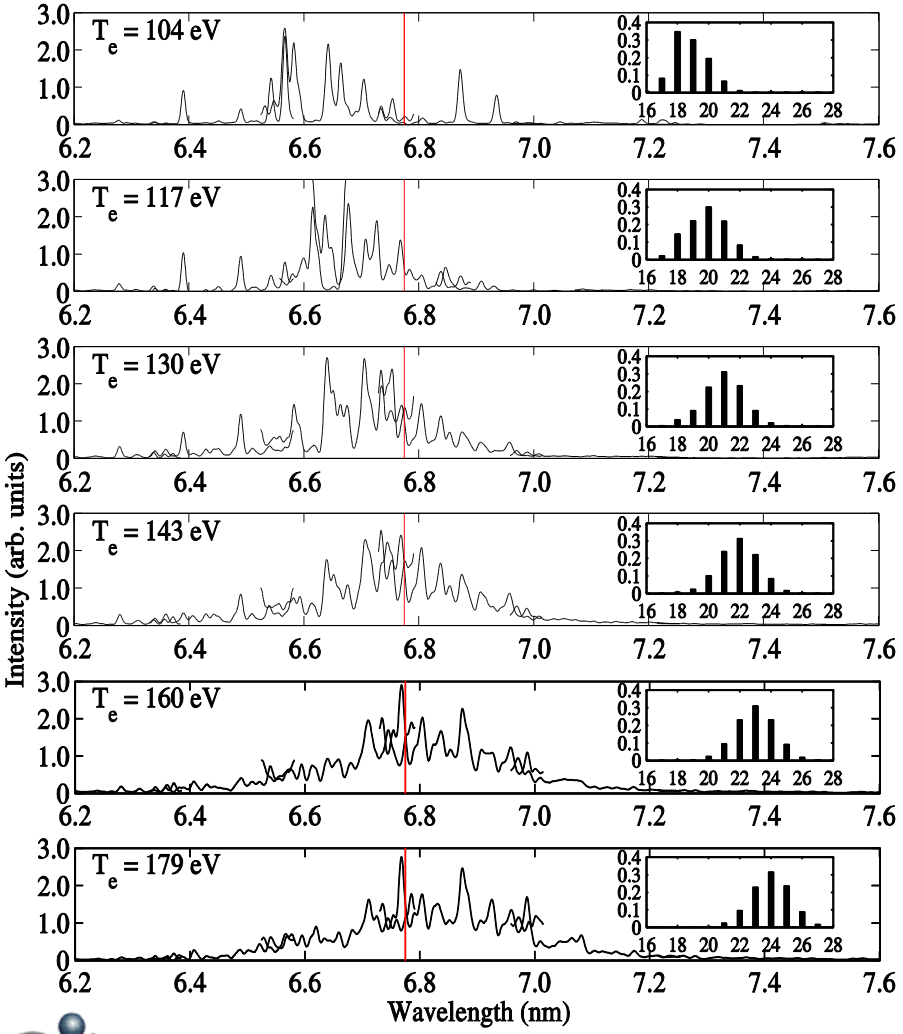

Calculations more complex than for Sn because of open 4f subshell in ions lower than 18+

In low stages, 4f, 5p and 4f, 5s level crossings give rise to very complex interacting configurations

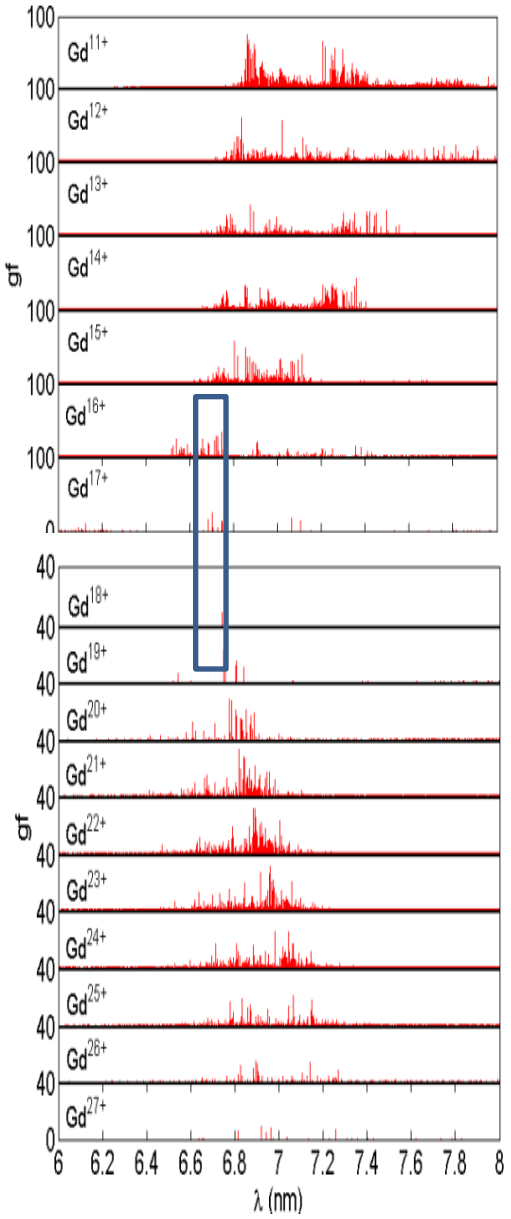

Power Density Requirements

Ion populations and average ionization of a Gd plasma as a function of T_e computed with the Collisional Radiative (CR) model. Most important stages are Ag-, Pd- and Rh- like (17+ - 19+)

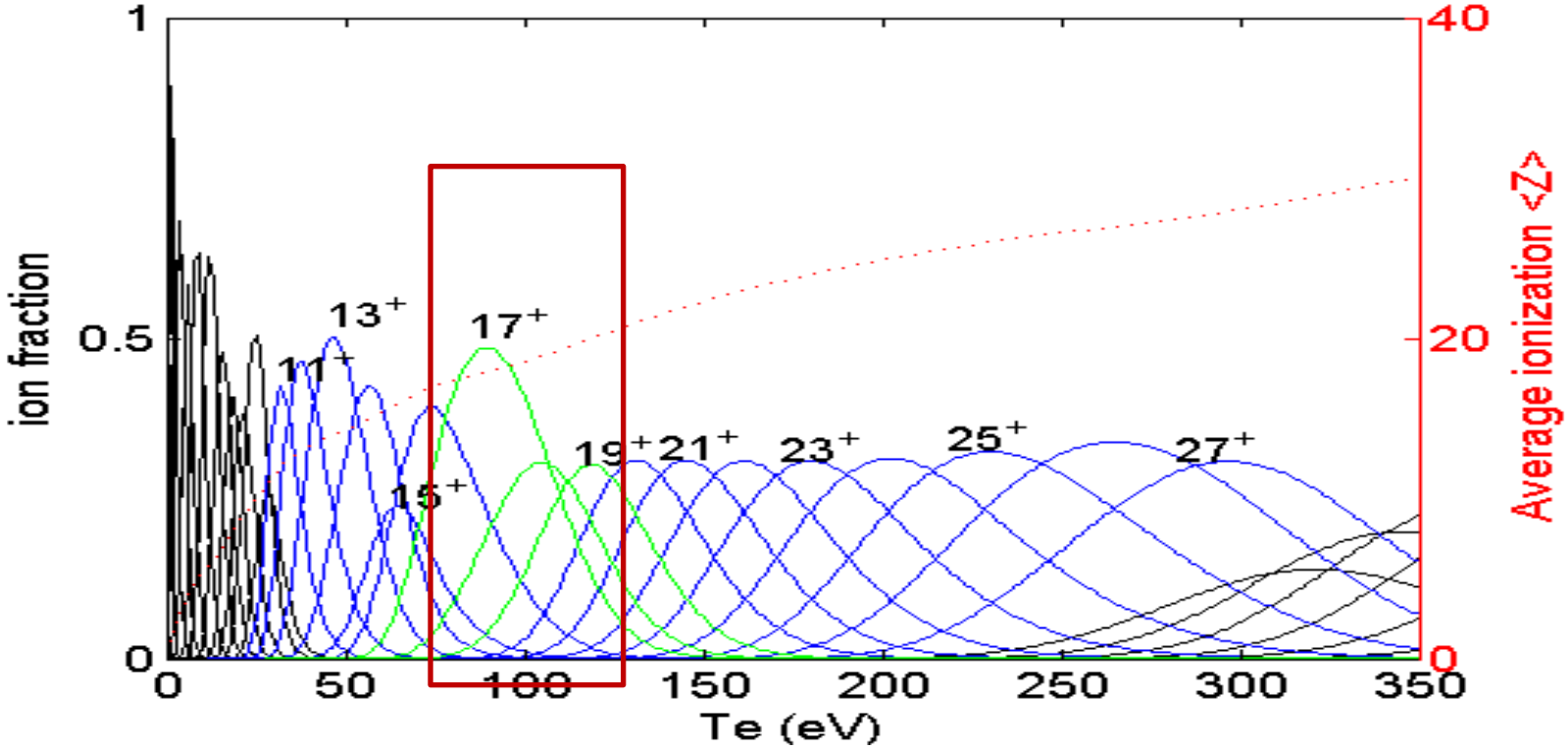

The laser power density required lies in the range

$2 \times 10^{12} - 10^{13}$ Wcm^{-2} @λ =1.06 μm

$2 \times 10^{11} - 10^{12}$ Wcm^{-2} @λ =10.6 μm

CO_2 vs Nd:YAG for drive laser

1-D Hydro modeling – demonstrated increase in CE for CO_2

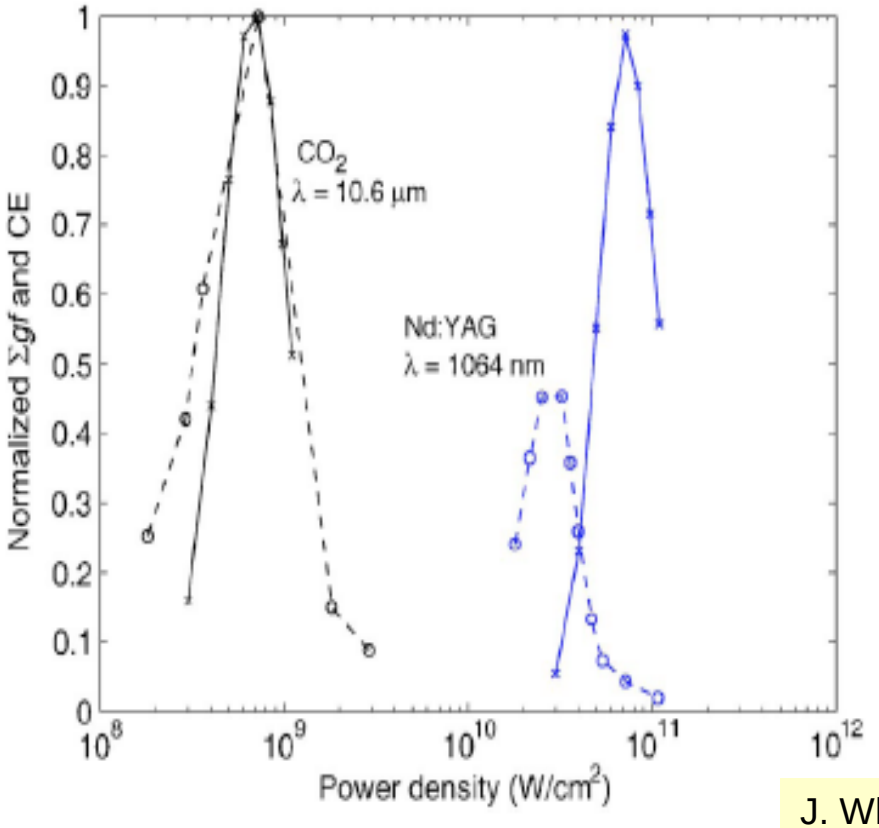

- **Lower power density required**
- **Less energy → better CE**
- **Improved opacity**

$n_{ec} \approx 10^{21} \lambda^{-2}$ (cm^{-3})

1064 nm: $n_{ec} \approx 1x10^{21}$ cm^{-3}
10600 nm: $n_{ec} \approx 1x10^{19}$ cm^{-3}

J. White et al, *Appl. Phys. Lett.*, **90**, 181502 (2007)

Variation of UTA with plasma temperature (Gd)

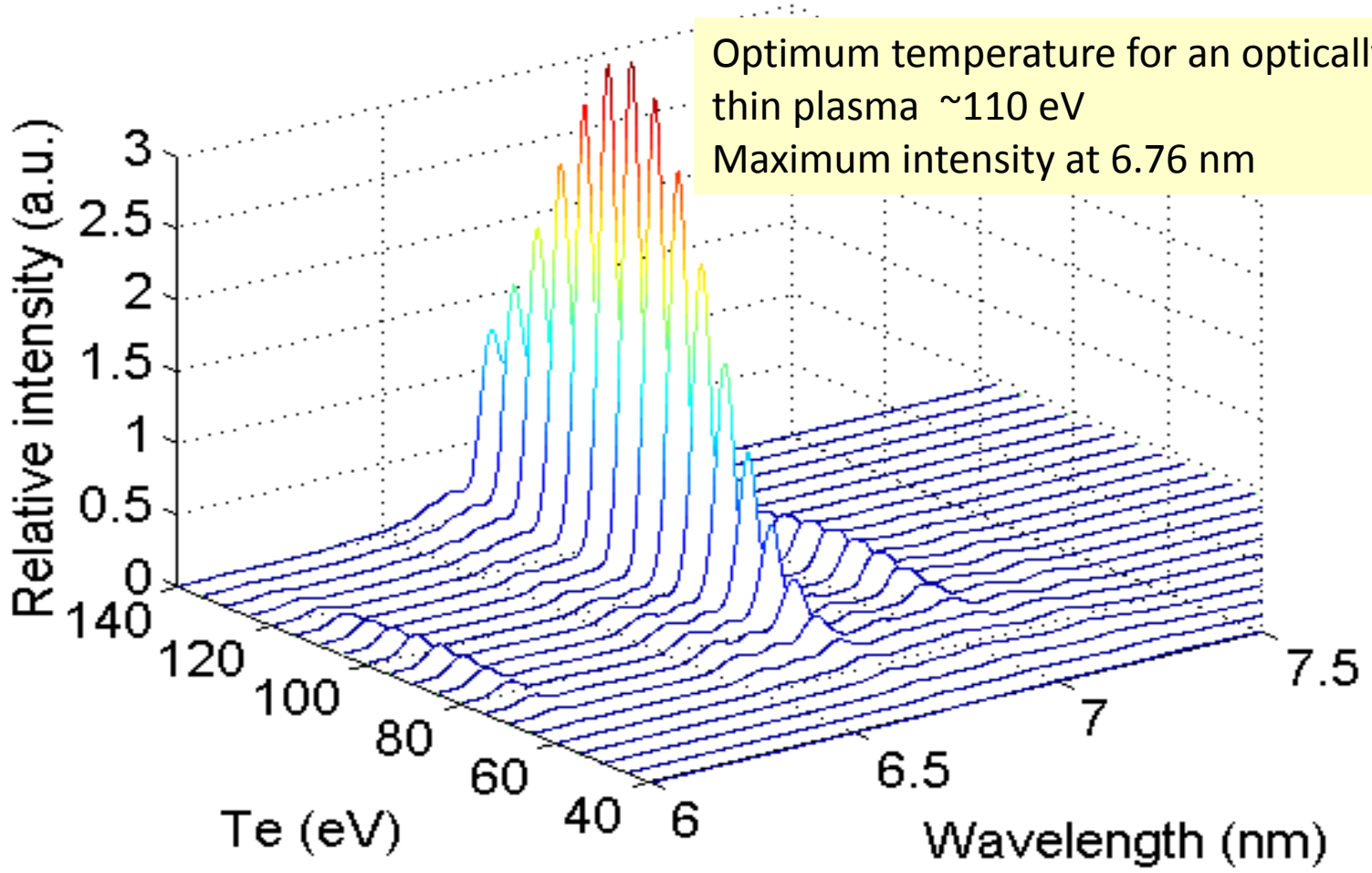

Optimum temperature for an optically thin plasma ~110 eV
Maximum intensity at 6.76 nm

Laser wavelength and target concentration effects

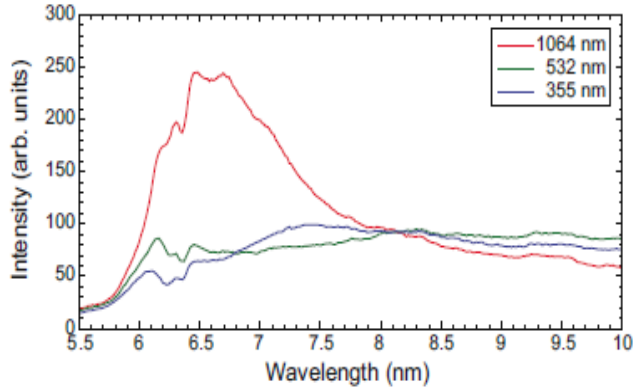

FIG. 1. (Color online) EUV spectra at laser wavelengths of 1064 (red), 532 (green), and 355 nm (blue) for the same laser intensity of 1.6 $\times 10^{12}$ W/cm^2 [laser energy: 320 mJ per pulse; spot diameter: 50 μm (FWHM)], respectively.

APPLIED PHYSICS LETTERS **97**, 231503 (2010)

Systematic investigation of self-absorption and conversion efficiency of 6.7 nm extreme ultraviolet sources

Takamitsu Otsuka,[1,a)] Deirdre Kilbane,[2] Takeshi Higashiguchi,[1,b)] Noboru Yugami,[1] Toyohiko Yatagai,[1] Weihua Jiang,[3] Akira Endo,[4] Padraig Dunne,[2] and Gerry O'Sullivan[2]
[1]*Department of Advanced Interdisciplinary Sciences and Center for Optical Research and Education (CORE), Utsunomiya University, Yoto 7-1-2, Utsunomiya, Tochigi 321-8585, Japan*
[2]*School of Physics, University College Dublin, Belfield, Dublin 4, Ireland*
[3]*Department of Electrical Engineering, Nagaoka University of Technology, Kami-tomiokamachi 1603-1, Nagaoka, Niigata 940-2188 Japan*
[4]*Forschungszentrum Dresden, Bautzner Landstrs. 400, Dresden D-01328, Germany*

APPLIED PHYSICS LETTERS **97**, 111503 (2010)

Rare-earth plasma extreme ultraviolet sources at 6.5–6.7

Takamitsu Otsuka,[1,a)] Deirdre Kilbane,[2] John White,[2] Takeshi Higashiguchi,[1,] Noboru Yugami,[1] Toyohiko Yatagai,[1] Weihua Jiang,[3] Akira Endo,[4] Padraig Du Gerry O'Sullivan[2]
[1]*Department of Advanced Interdisciplinary Sciences, Center for Optical Research & Educati Utsunomiya University, Yoto 7-1-2, Utsunomiya, Tochigi 321-8585, Japan*
[2]*School of Physics, University College Dublin, Belfield, Dublin 4, Ireland*
[3]*Department of Electrical Engineering, Nagaoka University of Technology, Kami-tomiokama Nagaoka, Niigata 940-2188, Japan*
[4]*Forschungszentrum Dresden, Bautzner Landstrs. 400, D-01328 Dresden, Germany*

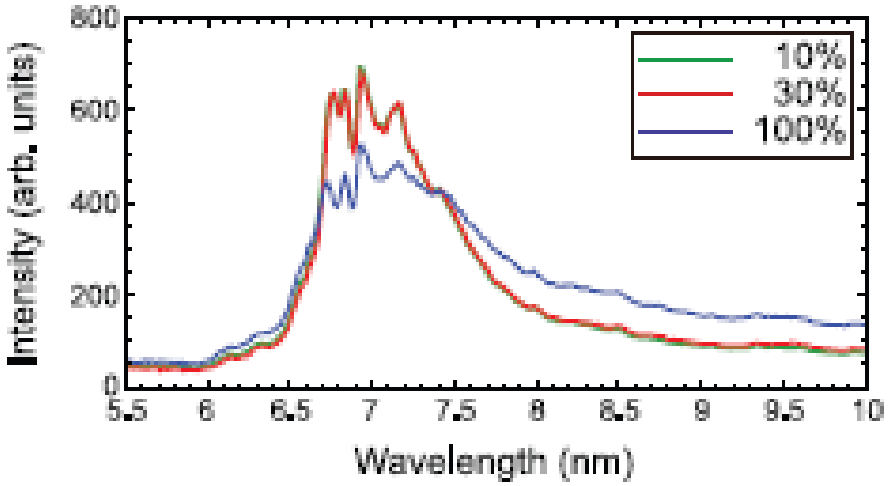

Effect of prepulses

Dual laser pulses of 8 ns and 10 ns (FWHM) at 532 nm and 1064 nm provided as pre- and main (at 5.6×10^{12} W/cm^2) laser pulses, respectively.

Pulse separation time dependence on the EUV CE on targets containing 30% (red, circles) or 100% Gd (blue, rectangles). The dashed lines correspond the single pulse illumination.

APPLIED PHYSICS LETTERS 99, 191502 (2011)

Extreme ultraviolet source at 6.7 nm based on a low-density plasma

Takeshi Higashiguchi,[1,2,a)] Takamitsu Otsuka,[1] Noboru Yugami,[1,2] Weihua Jiang,[3] Akira Endo,[4] Bowen Li,[5] Deirdre Kilbane,[5] Padraig Dunne,[5] and Gerry O'Sullivan[5]
[1]*Department of Advanced Interdisciplinary Sciences, Center for Optical Research & Education (CORE), and Optical Technology Innovation Center (OpTIC), Utsunomiya University, Yoto 7-1-2, Utsunomiya, Tochigi 321-8585 Japan*
[2]*Japan Science and Technology Agency, CREST, 4-1-8 Honcho, Kanagawa, Saitama 332-0012, Japan*
[3]*Department of Electrical Engineering, Nagaoka University of Technology, Kami-tomiokamachi 1603-1, Nagaoka, Niigata 940-2188 Japan*
[4]*Research Institute for Science and Engineering, Waseda University, Okubo 3-4-1, Shinjuku, Tokyo 169-8555, Japan*
[5]*School of Physics, University College Dublin, Belfield, Dublin 4, Ireland*

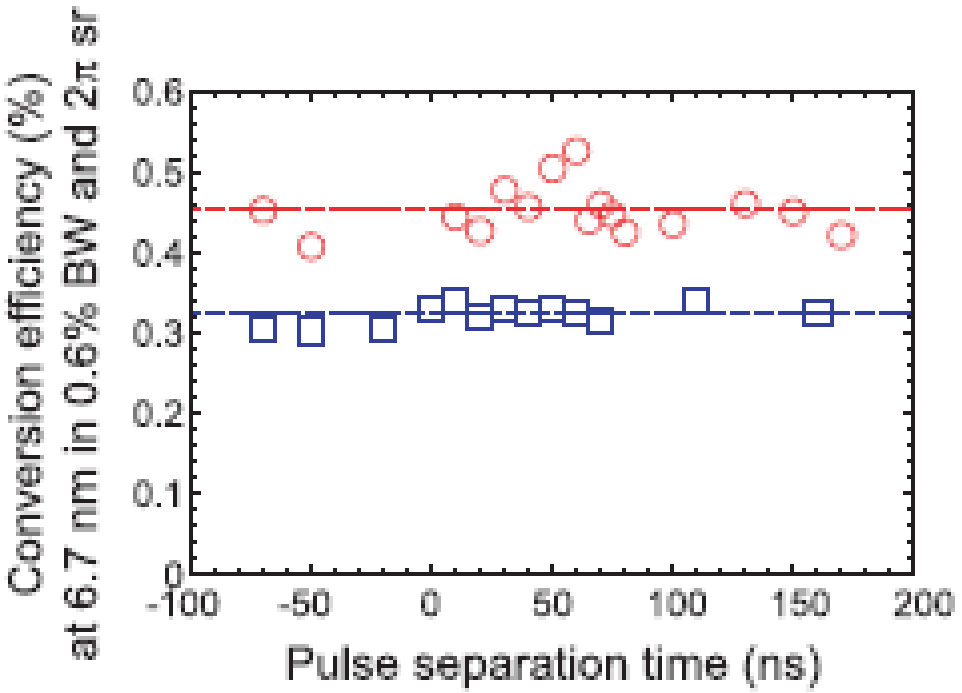

Effect of pulse duration

APPLIED PHYSICS LETTERS 100, 061118 (2012)

Optimizing conversion efficiency and reducing ion energy in a laser-produced Gd plasma

Thomas Cummins,[1,a)] Takamitsu Otsuka,[2] Noboru Yugami,[2,3] Weihua Jiang,[4] Akira Endo,[5] Bowen Li,[1] Colm O'Gorman,[1] Padraig Dunne,[1] Emma Sokell,[1] Gerry O'Sullivan,[1] and Takeshi Higashiguchi[2,3]
[1]School of Physics, University College Dublin, Belfield, Dublin 4, Ireland

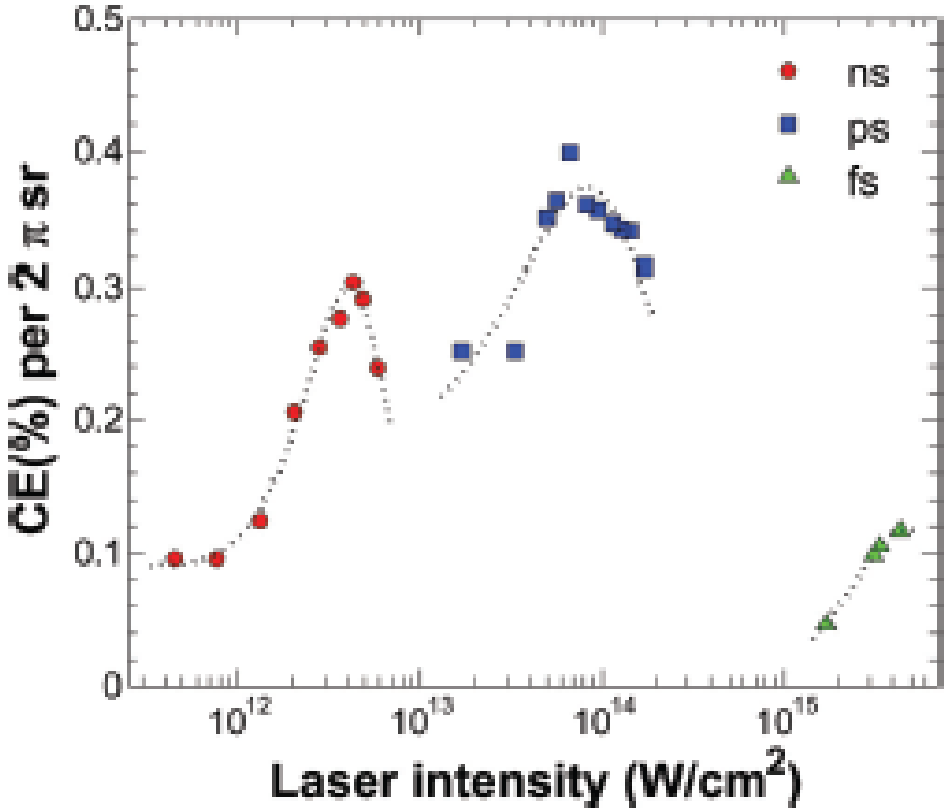

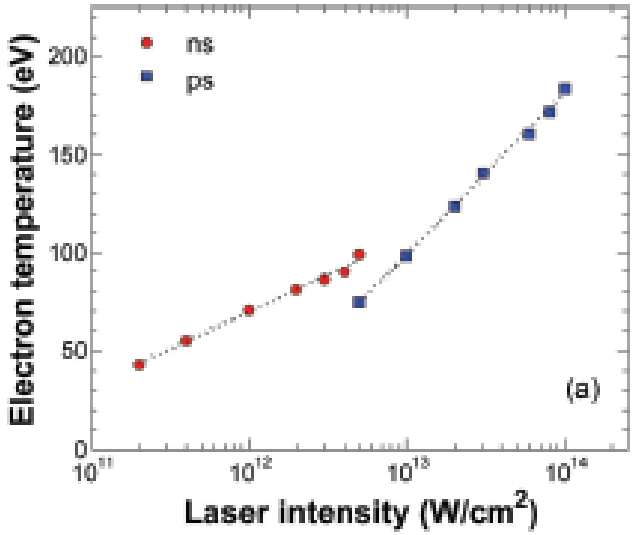

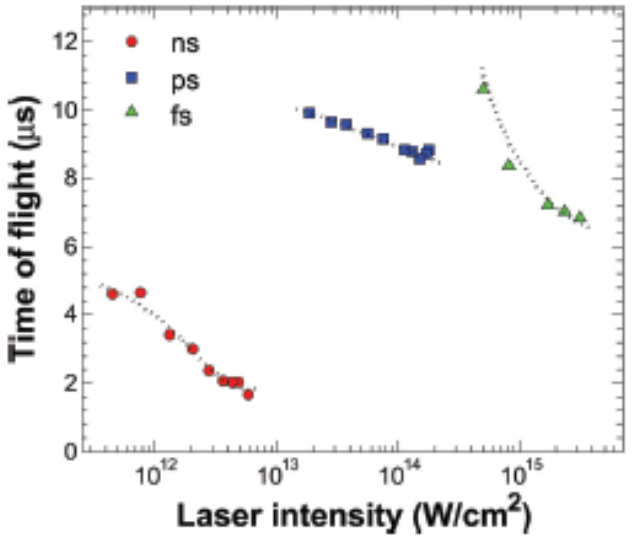

Water window source development

1. Motivation

Water Window: 2.3–4.4 nm. In this region, the absorption of carbon is approximately 10 times higher than that of oxygen and water.

Water window transmission X-ray microscope (WW-TXM): capable of yielding high resolution, high contrast images of carbon structures within biological specimens.

Potential Commercial Uses: ideally suited for investigations in the medical and microbiological research areas especially in DNA and RNA research, as well as in cancer and AIDS research.

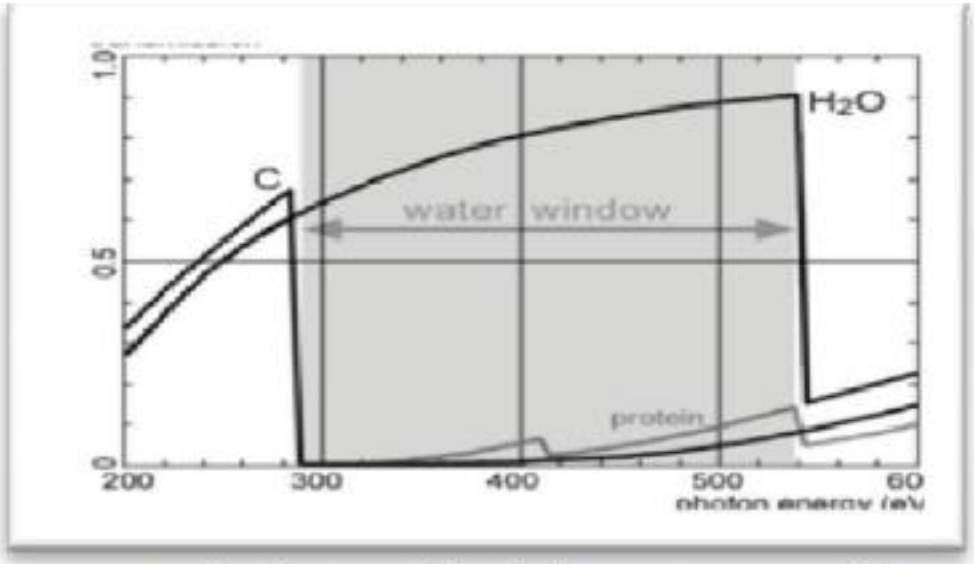

Fig. 1: *A plot of water and carbon's transmission coefficients in the water window region*

Simulation for Bi UTA

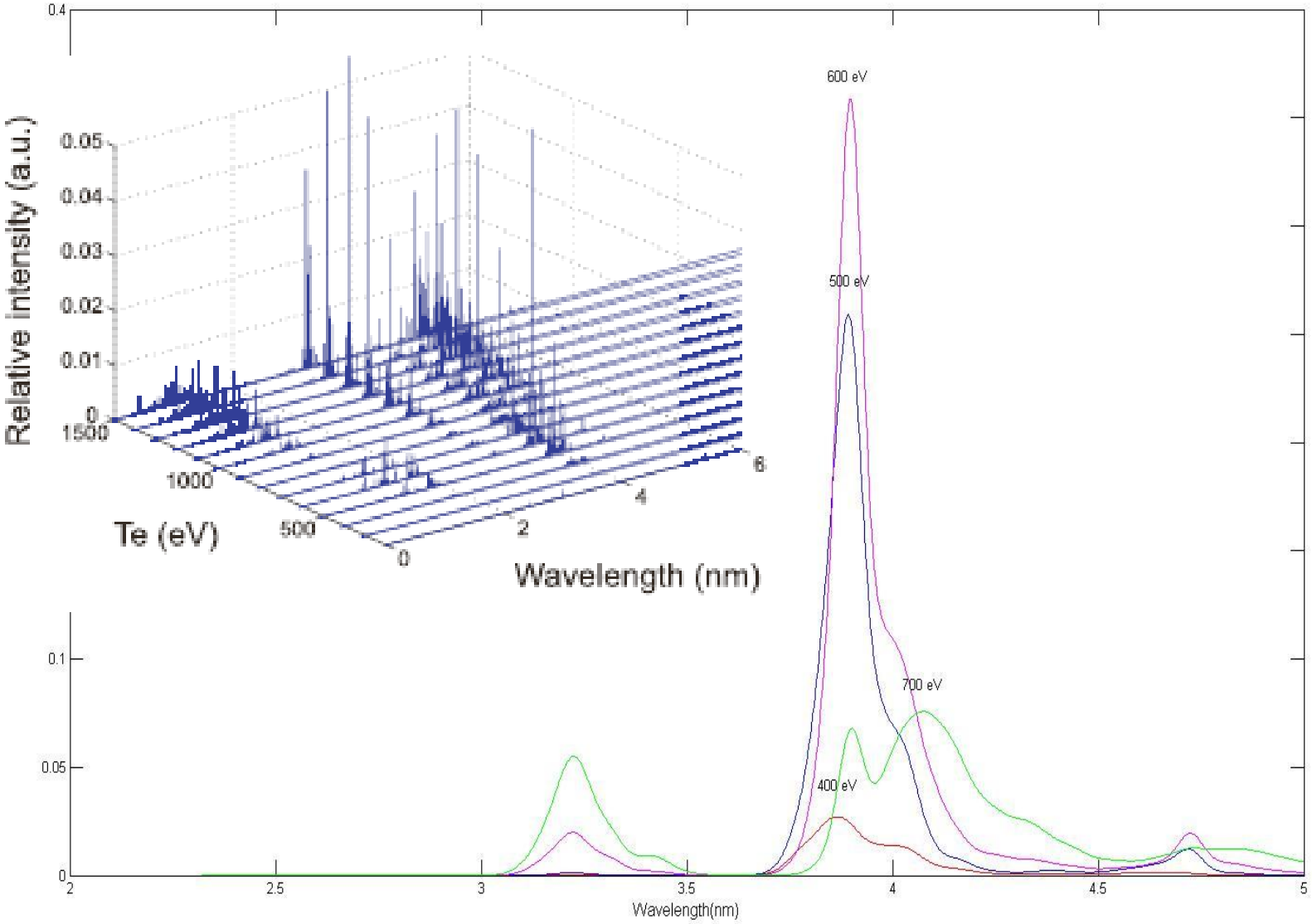

High temperature simulation

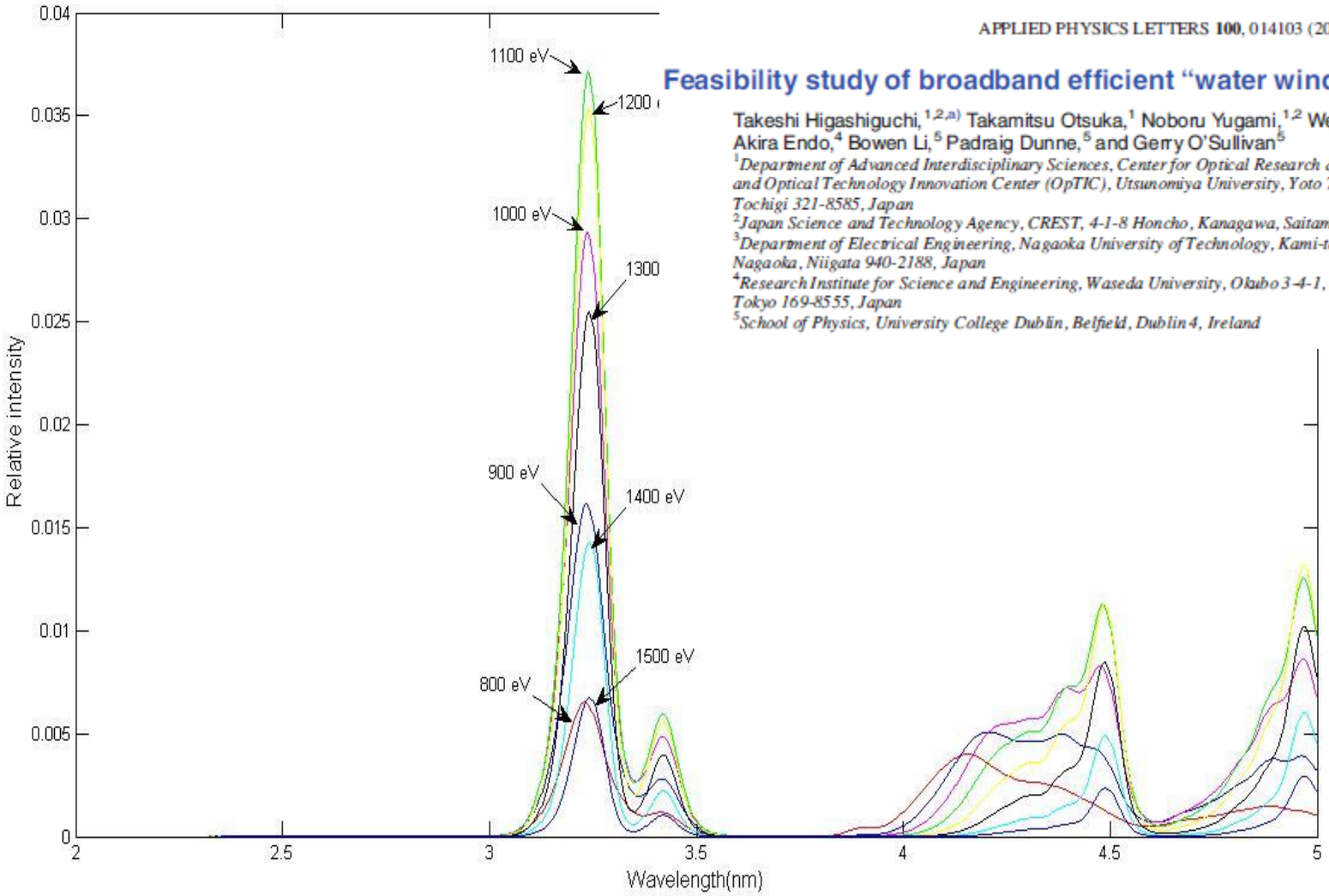

APPLIED PHYSICS LETTERS **100**, 014103 (2012)

Feasibility study of broadband efficient "water window" source

Takeshi Higashiguchi,[1,2,a)] Takamitsu Otsuka,[1] Noboru Yugami,[1,2] Weihua Jiang,[3] Akira Endo,[4] Bowen Li,[5] Padraig Dunne,[5] and Gerry O'Sullivan[5]

[1]*Department of Advanced Interdisciplinary Sciences, Center for Optical Research & Education (CORE), and Optical Technology Innovation Center (OpTIC), Utsunomiya University, Yoto 7-1-2, Utsunomiya, Tochigi 321-8585, Japan*

[2]*Japan Science and Technology Agency, CREST, 4-1-8 Honcho, Kanagawa, Saitama 332-0012, Japan*

[3]*Department of Electrical Engineering, Nagaoka University of Technology, Kami-tomiokamachi 1603-1, Nagaoka, Niigata 940-2188, Japan*

[4]*Research Institute for Science and Engineering, Waseda University, Okubo 3-4-1, Shinjuku, Tokyo 169-8555, Japan*

[5]*School of Physics, University College Dublin, Belfield, Dublin 4, Ireland*

- Background and underlying theory
- Properties and applications of $\Delta n = 0$ arrays
- Properties of and applications $\Delta n = 1$ arrays
- Conclusion

Other water window emission

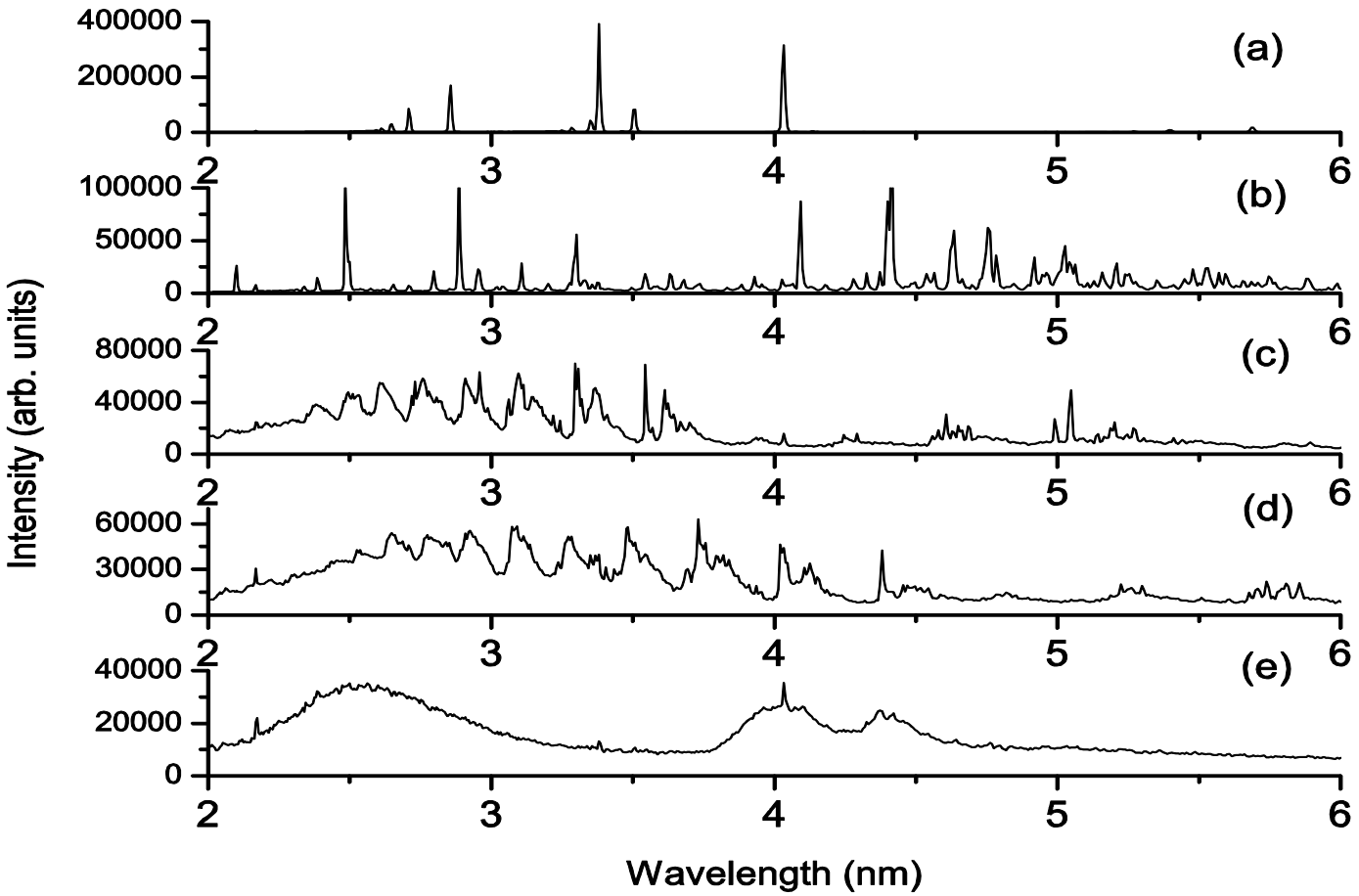

Time-integrated spectra from picosecond-laser-produced plasmas by use of C (a), Si_3N_4 (b), Mo (c), Zr (d) and Bi (e).

Δn = 1 3d-4f and 3d-4p UTA emission from Zr

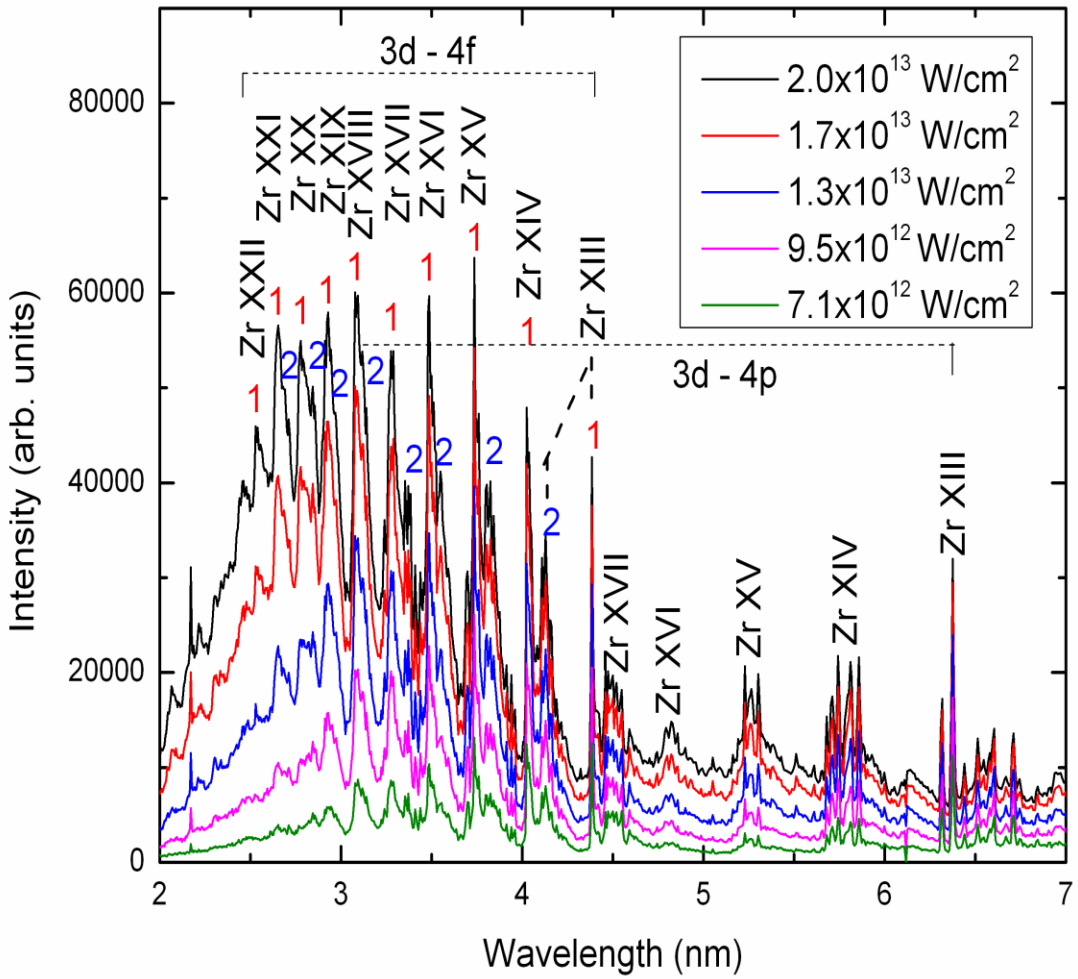

Spectral behavior of Zr plasmas as a function of laser laser intensity

Resonant $3d–4f$ (1) and $3d–4p$ transitions as well as satellite lines from $3d^{n-1}4s4f–3d^{n-2}4s4f$ (2)

Total number of counts in water window

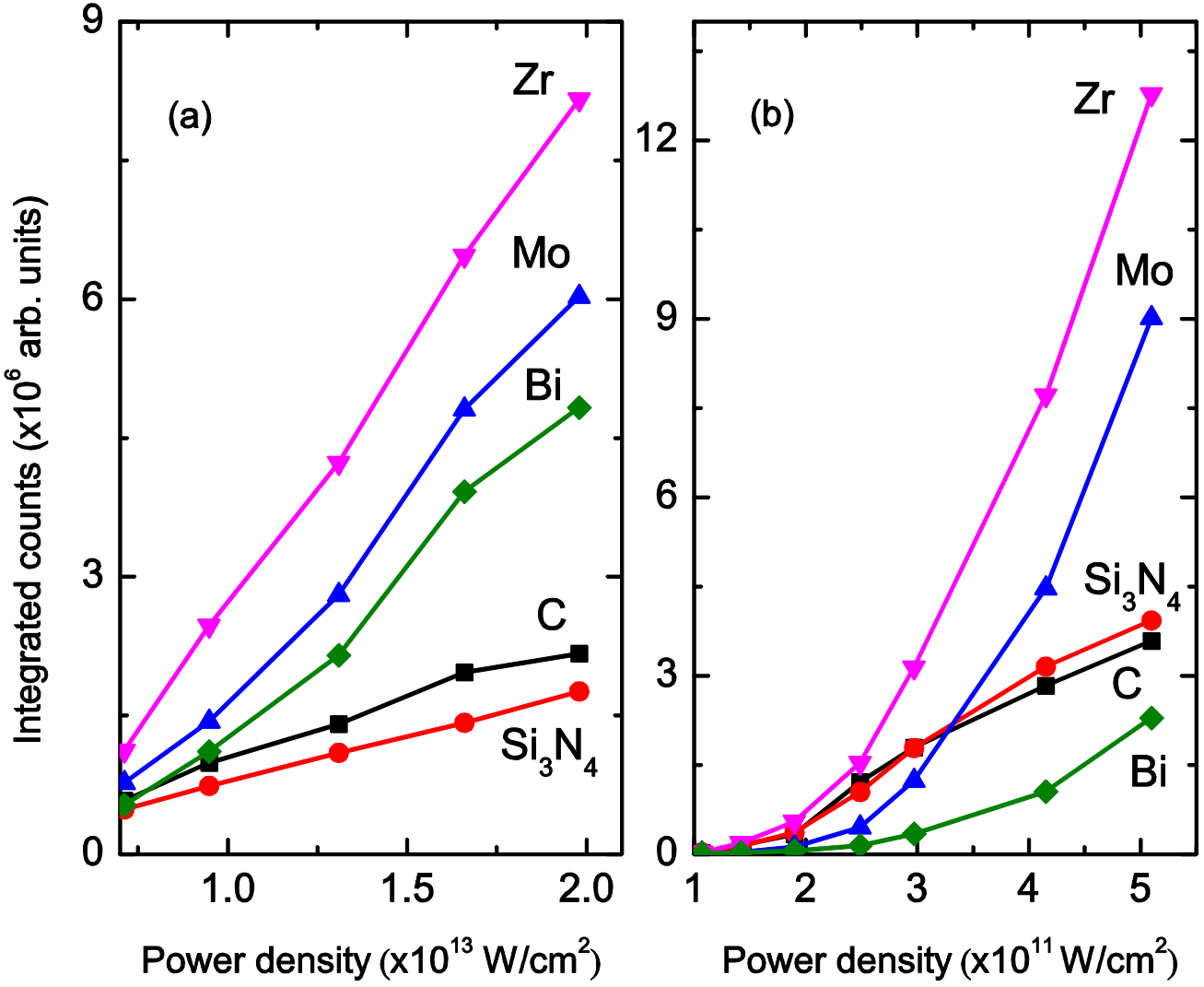

Water window emission (total counts) as a function of power density for ps (a) and ns (b) lasers

Effects of mirror bandwidth

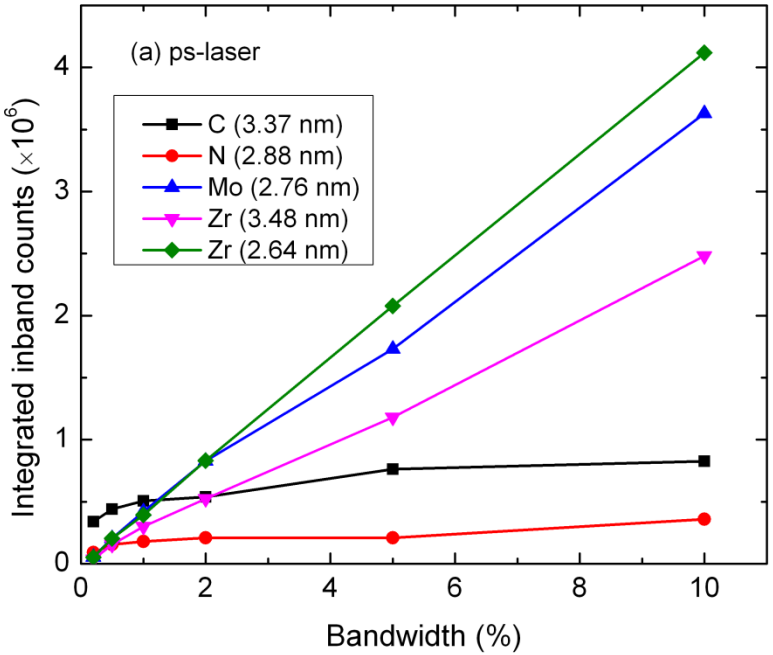

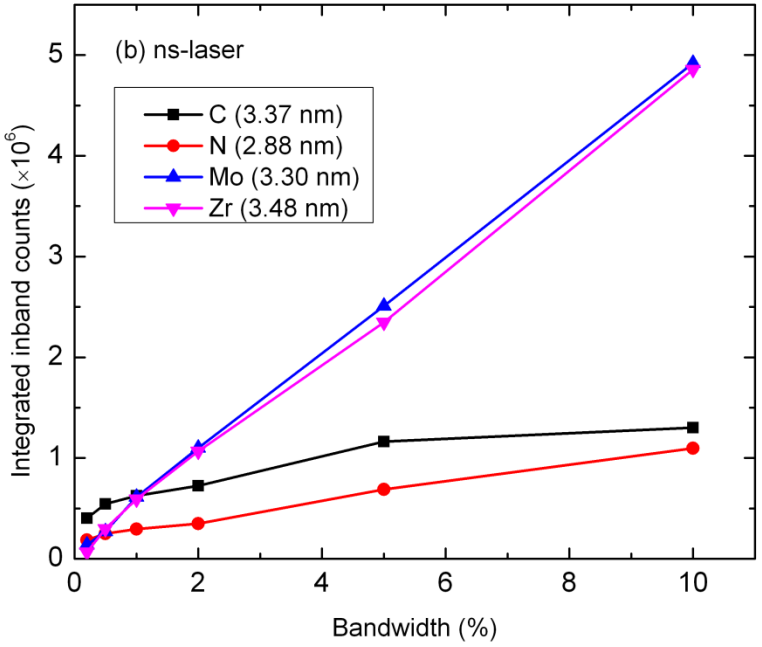

Integrated in-band counts against bandwidth (0.5%, 1%, 2%, 5% and 10%) for ps (a) and ns (b) laser.

Optimum wavelength

The optimum wavelength for Zr are 34.83 Å for ns-laser and 26.42 Å for ps-laser.

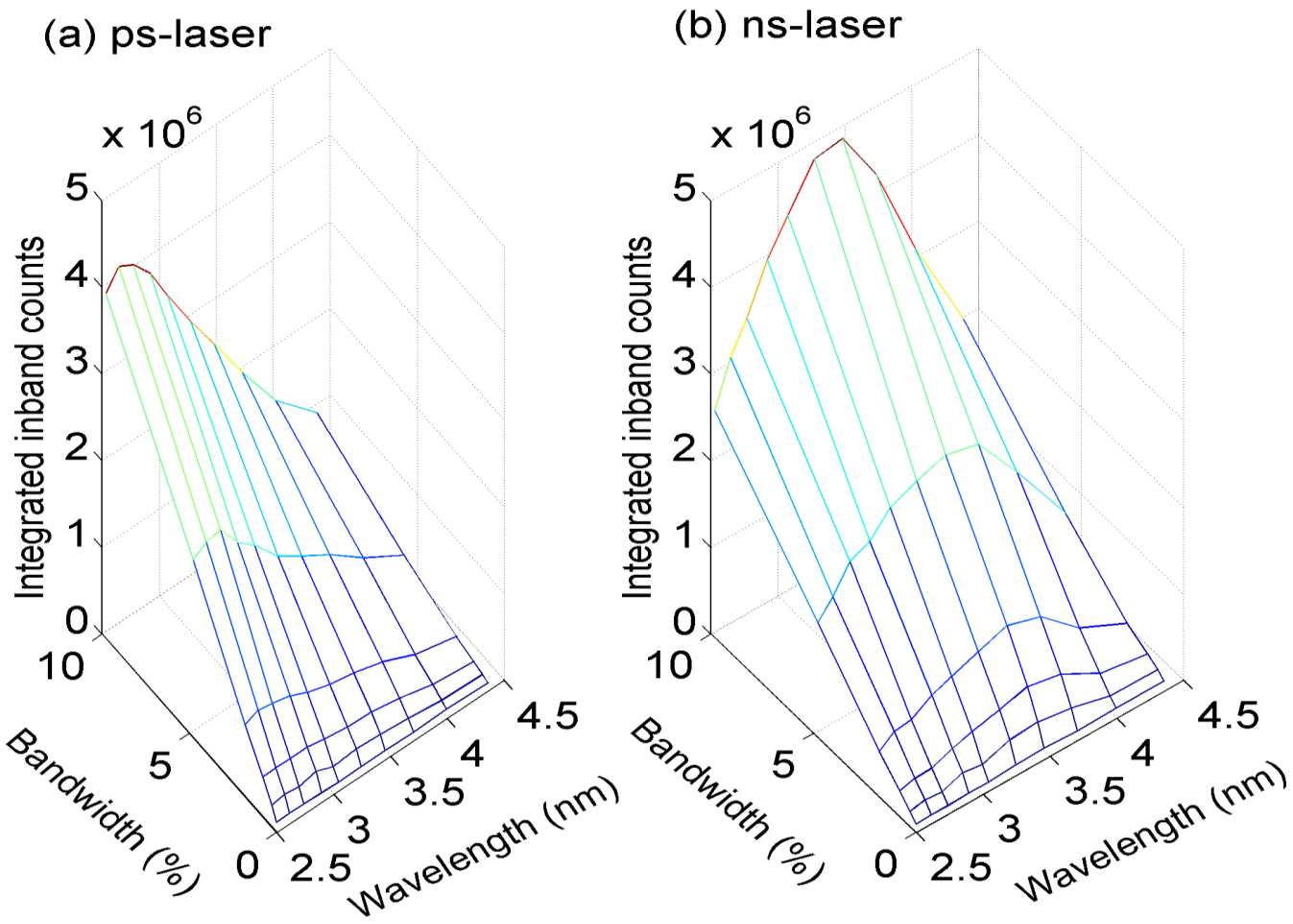

Integrated in-band counts for each peak of Zr against bandwidth for ps (a) and ns (b) laser.

Atomic Processes in Zr

In equilibrium:

$$\frac{dN(k)}{dt} = R^{DC}(i)N_eN(i) + R^{EIE}(j,k)N_eN(j) - (R^{DE}(k,j)N_e + A^r(k,j) + A^a(k,i))N(k)$$
$$= 0$$

Atomic processes related to $3d^94s4f$ state.

- DC, dielectronic capture;
- EIE, Electron-impact excitation;
- DE, de-excitation.
- calculated autoionisation (A^a) and radiative transition (A^r) rates are 1.31×10^{14} s^{-1} and 7.52×10^{12} s^{-1}, respectively

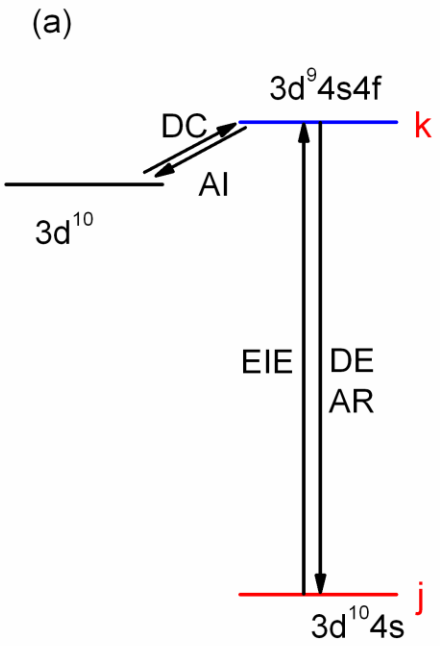

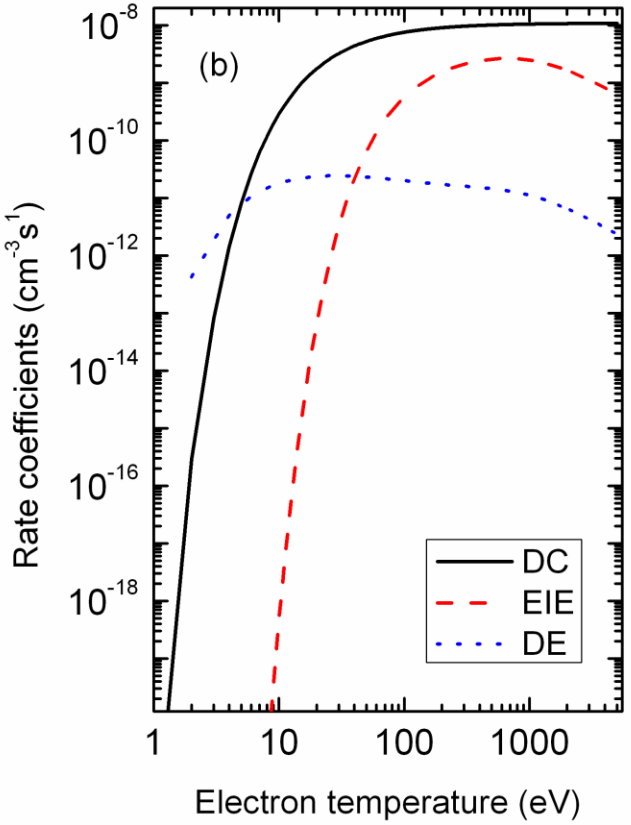

Level structure of Zr ions

Energy-level diagram showing in ascending order the level structure of $3d^n$, $3d^{n-1}$ (4s, 4p, 4f), and $3d^{n-2}$ 4s(4p, 4f) configurations for each ion stage

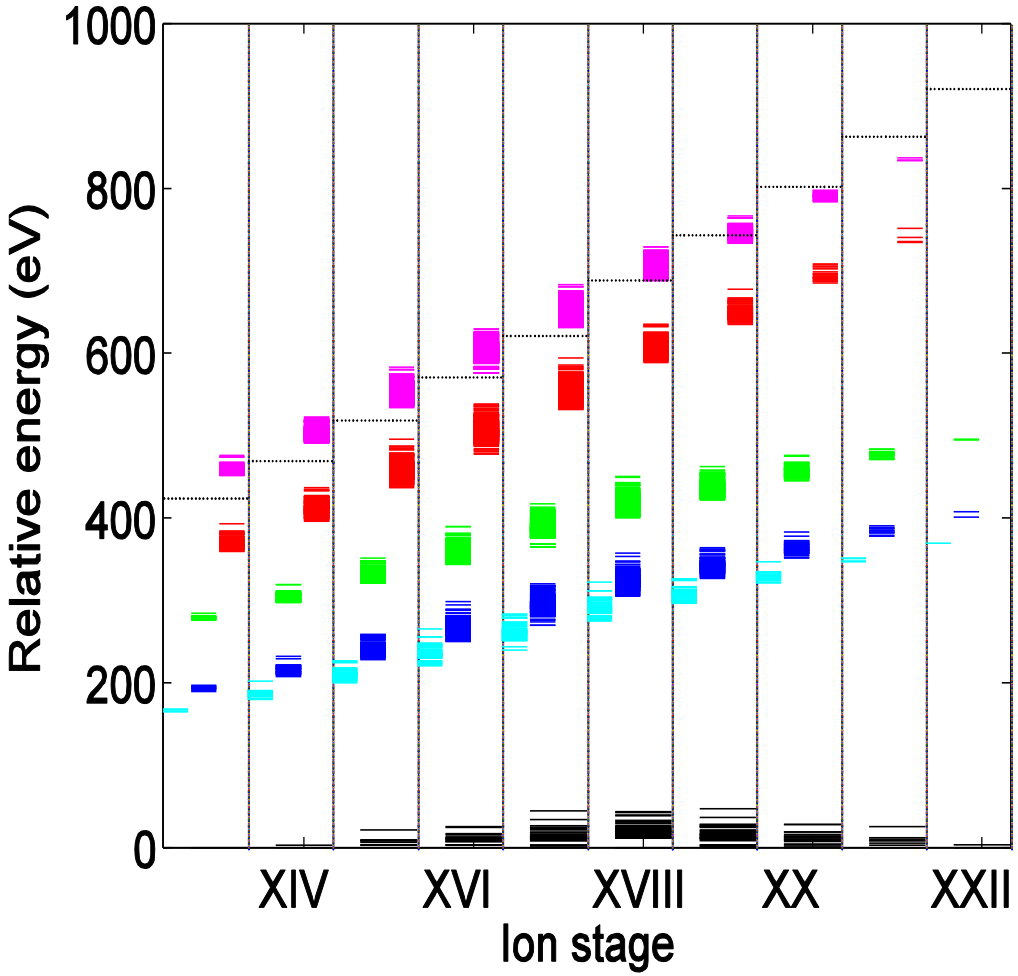

Comparison of calculation with experiment

Comparison between the observed spectrum and numerically calculated spectra with and without satellite lines assuming a steady-state CR model for different plasma temperatures of 100 (a), 150 (b), and 200 eV (c).

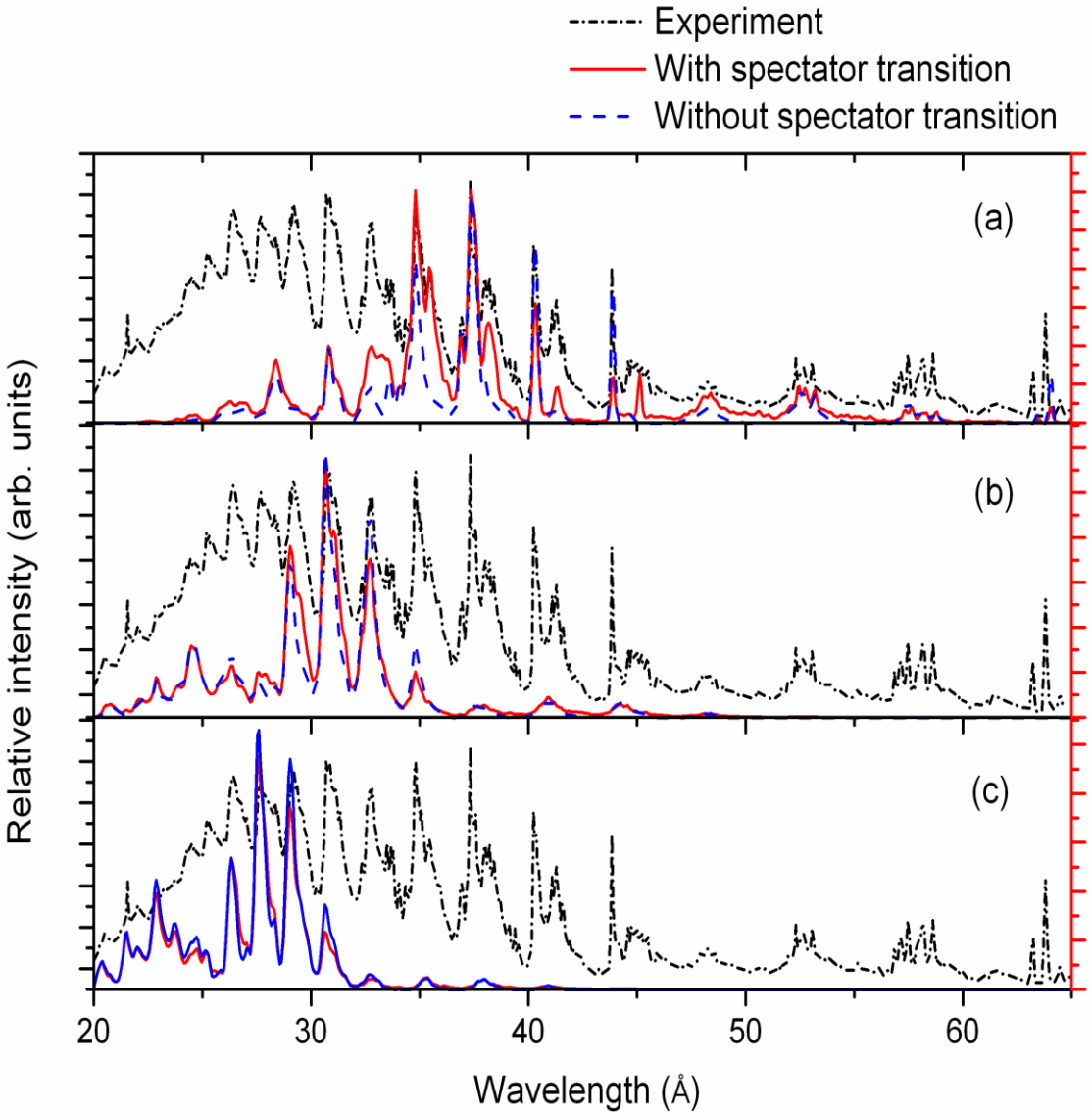

Conclusion

- $\Delta n = 0$ transitions extendable for 6.x and SXR source development
- For $\Delta n = 0$ transitions, maximum brightness in LPPs if $n_{ion} < 10^{18}$ $cm^{-3} \rightarrow$ CO_2 lasers or low density targets.
- $\Delta n = 1$ transitions may be useful with narrow bandwidth reflectors at short wavelengths for WW source development.

Acknowledgements

Science Foundation Ireland
Principal Investigator Grant
07/IN1/I1771

EU Marie Curie IAPP Project
FIRE

EU COST Action MP0601

Thank You!